

MINIMALISTIC UNSUPERVISED LEARNING WITH THE SPARSE MANIFOLD TRANSFORM

Yubei Chen^{1,2}, Zeyu Yun^{4,5}, Yi Ma⁴, Bruno Olshausen^{4,5,6}, Yann LeCun^{1,2,3}

¹ Meta AI

² Center for Data Science, ³ Courant Inst., New York University

⁴ EECS Dept., ⁵ Redwood Center, ⁶ Helen Wills Neuroscience Inst., UC Berkeley

ABSTRACT

We describe a minimalistic and interpretable method for unsupervised learning, without resorting to data augmentation, hyperparameter tuning, or other engineering designs, that achieves performance close to the SOTA SSL methods. Our approach leverages the sparse manifold transform [20], which unifies sparse coding, manifold learning, and slow feature analysis. With a one-layer deterministic sparse manifold transform, one can achieve 99.3% KNN top-1 accuracy on MNIST, 81.1% KNN top-1 accuracy on CIFAR-10 and 53.2% on CIFAR-100. With a simple gray-scale augmentation, the model gets 83.2% KNN top-1 accuracy on CIFAR-10 and 57% on CIFAR-100. These results significantly close the gap between simplistic “white-box” methods and the SOTA methods. Additionally, we provide visualization to explain how an unsupervised representation transform is formed. The proposed method is closely connected to latent-embedding self-supervised methods and can be treated as the simplest form of VICReg. Though there remains a small performance gap between our simple constructive model and SOTA methods, the evidence points to this as a promising direction for achieving a principled and white-box approach to unsupervised learning.

1 INTRODUCTION

In the past few years, there has been tremendous progress in the unsupervised representation learning community. This trend promises unparalleled scalability for data-driven machine learning in the future. However, while we are celebrating the empirical advancements, the question of what a learned representation is and how exactly it is formed in an unsupervised fashion is still unclear. Furthermore, it remains unclear whether there exists a set of common principles underlying all these unsupervised representations.

Many investigators have realized the importance of improving our understanding and have made pioneering steps trying to simplify the SOTA methods [17; 18; 104; 21], to establish the connections to classical methods [65; 3], to unify different approaches [3; 37; 89; 58; 52], to visualize the representation [8; 106; 14], and to analyze the methods from a theoretical perspective [2; 43; 98; 3]. The hope is that such understanding will lead to a theory that enables us to build simple, fully explainable, “white-box” models [13; 12] from data based on first principles. Such a computational theory could also provide guidance in understanding the principles governing unsupervised learning in the human brain [77; 29; 30; 61].

In this work, we make a small step toward this goal by trying to build a minimalistic “white-box” unsupervised learning model without deep networks, projection heads, augmentation, or various other engineering designs. By leveraging two classical unsupervised learning principles, sparsity [75; 76] and spectral embedding [82; 96], we build a two-layer model which achieves non-trivial benchmark results on several standard datasets. In particular, we show that a two-layer model based on the sparse manifold transform [20], which shares the same objective as latent-embedding SSL methods [4], achieves 99.3% KNN top-1 accuracy on MNIST, 81.1% KNN top-1 accuracy on CIFAR-10, and 53.2% on CIFAR-100 without any data augmentation. With a simple grayscale augmentation, it achieves 83.2% KNN top-1 accuracy on CIFAR-10 and 57% KNN top-1 accuracy on CIFAR-100.

These results make a step to close the gap between a “white-box” model and the SOTA SSL models [17; 19; 4; 107]. Though the gap is still clear, we argue that further closing it can potentially lead to a deeper understanding of unsupervised representation learning, and this is a promising path towards a useful theory.

We first begin the technical discussion below by addressing three fundamental questions. Then in Section 2, we revisit the formulation of SMT and discuss how it is used to solve various unsupervised learning problems. In Section 3, we present the benchmark results on MNIST, CIFAR-10, and CIFAR100, together with visualization and ablations for a better understanding. Further related literature is discussed in Section 4. Finally, we make additional discussion in Section 5.

Three fundamental questions:

What is an unsupervised (self-supervised) re-representation? Essentially, any non-identity transformation of the original signal can be called a re-representation. However, it is the useful ones that are interesting. One general goal in unsupervised re-representation learning is to find a function that transforms raw data into a new space such that “similar” things are placed closer to each other. Meanwhile, the new space should not be a collapsed trivial one¹, i.e., the important geometric or stochastic structure of the data must be preserved. If this goal is achieved, then naturally “dissimilar” things would be placed far apart in the representation space.

Where does “similarity” come from? “Similarity” comes from three classical ideas, which were proposed multiple times in different contexts: 1) temporal co-occurrence [102], 2) spatial co-occurrence [83; 26; 32; 78], and 3) local neighborhoods [82; 96] in the raw signal space. These ideas overlap to a considerable extent when the underlying structure is geometric², but they can also conceptually differ when the structure is stochastic. In Figure 1, we illustrate the difference between a manifold structure and a stochastic co-occurrence structure. Leveraging these localities, two unsupervised learning methods emerge from these ideas: manifold learning and co-occurrence statistics modeling. Interestingly, many of these ideas reach a spectral decomposition formulation or a closely related matrix factorization formulation [102; 82; 96; 25; 51; 42; 79; 44; 20].

The philosophy of manifold learning is that only local neighborhoods in the raw signal space can be trusted, and the global geometry emerges by considering all the local neighborhoods together, i.e. “think globally, fit locally” [85]. In contrast, co-occurrence statistics modeling bears a probabilistic view, which complements the manifold view as some structures cannot be modeled by continuous manifolds. The most prominent example comes from natural languages, where the raw data hardly comes from a smooth geometry. In word embedding [71; 72; 79], “Seattle” and “Dallas” may reach a similar embedding though they do not co-occur the most frequently. The underlying reason is that they share similar context patterns [64; 108]. The probabilistic and manifold points of view complement each other for understanding “similarity”. Now we have a proper definition of similarity; the next step is to construct a non-trivial transform such that similar things are placed closer.

How do we establish the representation transform? The parsimonious principles: sparsity and low rank. The general idea is that we can use sparsity to handle locality and decomposition in the data space to build a support. And then, we can construct our representation transform with low-frequency functions, which assign similar values to similar points on the support. This process is called *the sparse manifold transform* [20].

2 UNSUPERVISED LEARNING WITH THE SPARSE MANIFOLD TRANSFORM

The sparse manifold transform. The sparse manifold transform (SMT) was proposed to unify several fundamental unsupervised learning methods: sparse coding, manifold learning, and slow feature analysis. The basic idea of SMT is: 1) first to lift the raw signal x into a high-dimensional space by a non-linear sparse feature function f , i.e. $\vec{\alpha} = f(\vec{x})$, where locality and decomposition are respected. 2) then to linearly embed the sparse feature $\vec{\alpha}$ into a low-dimensional space, i.e., $\vec{\beta} = P\vec{\alpha}$, such that the similarity or “trajectory linearity” is respected. As we mentioned earlier, for

¹An obvious trivial solution is that we collapse every data point to a single point in the new space.

²If we consider the signals temporally or spatially co-occur are related by a smooth transformation, then these three ideas are equivalent.

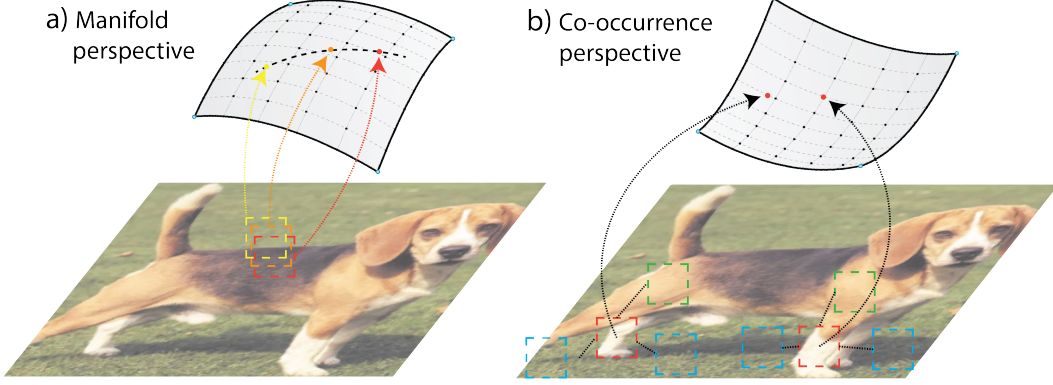


Figure 1: **Two different points of view.** (a) Manifold: There are three patches in the dashed boxes. Let’s assume there is a path between them on a manifold of the image patch space; then, their relationship can be found based on either the Euclidean neighborhoods, spatial co-occurrence, or temporal co-occurrence from smooth transformation. (b) Probabilistic: For the two red boxes (“leg”), it is unclear whether there is a path between them in the patch space. However, they can still be considered to be similar under spatial co-occurrence because they appear in the same context. These two patches both co-occur with the “grass land” (blue boxes) and “elbow or body” (green boxes). Temporal co-occurrence has a similar effect.

each data point x_i , we can choose to use either its local neighbors in the raw signal space, its spatial co-occurrence neighbors, or its temporal co-occurrence neighbors to define similarity. Let’s denote the neighbors of x_i as $x_{n(i)}$, the optimization objective is the following:

$$\min_P \sum_i \sum_{j \in n(i)} \|P\tilde{\alpha}_i - P\tilde{\alpha}_j\|_F^2, \quad \text{s.t.} \quad P \mathbb{E}[\tilde{\alpha}_i \tilde{\alpha}_i^T] P^T = I \quad (1)$$

where $\tilde{\alpha} = f(\cdot)$ is a sparse feature extraction function, e.g. 1-sparse vector quantization f_{vq} and sparse coding f_{sc} . Later we will provide several other examples.

Similarity can be considered as a first-order derivative. A more restrictive requirement is linearity [82], which is the second-order derivative. Then the objective is changed to a similar one:

$$\min_P \sum_i \|P\tilde{\alpha}_i - \sum_{j \in n(i)} w(i, j) P\tilde{\alpha}_j\|_F^2, \quad \text{s.t.} \quad P \mathbb{E}[\tilde{\alpha}_i \tilde{\alpha}_i^T] P^T = I \quad (2)$$

where $\sum_{j \in n(i)} w(i, j) = 1$. Several ways to acquire $w(\cdot, \cdot)$ are: to use locally linear interpolation, temporal linear interpolation, or spatial neighbor linear interpolation. If we write the set $\{\tilde{\alpha}_i\}$ as a matrix A , where each column of A corresponds to the sparse feature of a data point, then both Optimization 1 and Optimization 2 can be formulated as the following general formulation [20]:

$$\min_P \|PAD\|_F^2, \quad \text{s.t.} \quad PVP^T = I \quad (3)$$

where D is a differential operator, $V = \frac{1}{N}AA^T$ and N is the total number of data point. D corresponds to a first-order derivative operator in Optimization 1 and a second-order derivative operator in Optimization 2. For Optimization 1, $D_{ji} = -1$ for $j \in n(i)$, $D_{ii} = |n(i)|$, and $D_{ji} = 0$ otherwise. For Optimization 2, $D_{ji} = -w(i, j)$ for $j \in n(i)$, $D_{ii} = 1$, and $D_{ji} = 0$ otherwise. The solution to this generalized eigen-decomposition problem is given [100] by $P = UV^{-\frac{1}{2}}$, where U is a matrix of f trailing eigenvectors (i.e. eigenvectors with the smallest eigenvalues) of the matrix $Q = V^{-\frac{1}{2}}ADD^T A^T V^{-\frac{1}{2}}$. Please note that if U contains all of the eigenvectors of Q , then the solution of SMT reduces to the whitening matrix. We can generalize f to an arbitrary function as long as it can capture the locality and structures in the signal space. If we choose f as a quadratic expansion function, Optimization 1 would reduce to slow feature analysis [102].

Manifold point of view: a 2D nonlinear manifold disentanglement problem. Let’s consider a spiral manifold disentanglement problem in a 2D space shown in Figure 2(a). As it is not a linearly-separable problem, to construct a representation function to disentangle the two spiral manifolds,

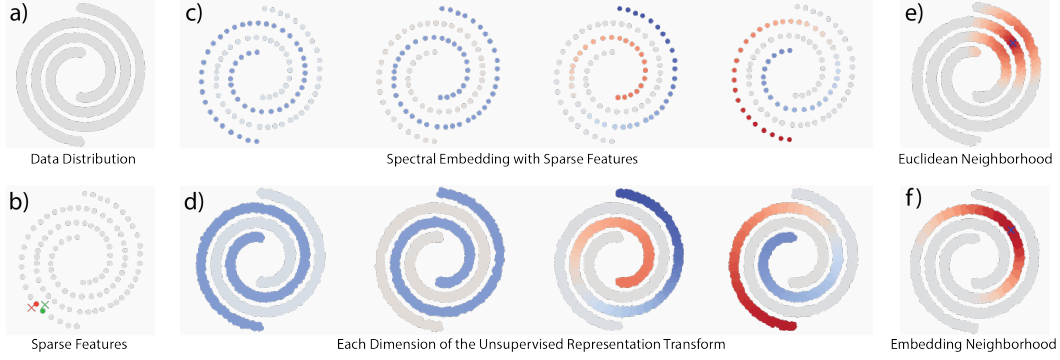


Figure 2: **Manifold disentanglement with SMT.** (a) Data distribution along two entangled 1D spiral manifolds in the 2D ambient space. (b) Sparse feature (dictionary) learned with 1-sparse sparse coding is shown as dots. They serve as a set of landmarks to tile the data manifolds. Given two points marked as red and green crosses, the 1-sparse feature function maps them to the corresponding dictionary element, marked as red and green dots. (c) Spectral embedding assigns similar values to nearby dictionary elements. Each embedding dimension is a low-frequency function defined on the sparse dictionary support. We show the first 4 embedding dimensions, i.e., the first 4 rows of P , $P_{1,\cdot}$, $P_{2,\cdot}$, $P_{3,\cdot}$, and $P_{4,\cdot}$. The color represents the projection values for each dictionary element. (d) The sparse manifold transform is a vector function $Pf(\cdot)$, and we plot the first four dimensions of SMT over the data distribution. The color represents the projection values for each data point. (e) We show the Euclidean neighborhood of the point marked by a blue cross in the original data space. (f) After the sparse manifold transform, we show the cosine similarity neighborhood of the point marked by the same blue cross in the representation space.

we need to leverage nonlinearity and give the transform function enough flexibility to respect the locality in the data space. Let's first use 1-sparse sparse coding to learn an overcomplete dictionary³, i.e. a set of K landmarks [90; 25], to tile the space. This dictionary serves as the support of the representation function, as shown in Figure 2(b). This dictionary turns a data point \vec{x} into a 1-sparse vector $\vec{\alpha} = f(\vec{x}) = \operatorname{argmin}_{\vec{\alpha}} \|\vec{x} - \Phi\vec{\alpha}\|$, s.t. $\|\vec{\alpha}\|_0 = 1$, $\|\vec{\alpha}\|_1 = 1$; $\vec{\alpha} \in \mathbb{R}^K$ is an 1-hot vector and denotes the closest dictionary element $\vec{\phi}$ to \vec{x} . Next, we seek a linear projection P to embed the sparse vector $\vec{\alpha}$ to a lower dimensional space, $\vec{\beta} = Pf(\vec{x})$ and $\vec{\beta} \in \mathbb{R}^d$, which completes the transform. Each column of $P \in \mathbb{R}^{d \times K}$ corresponds to a d -dimensional vectors assigned to the corresponding entry of α . The i^{th} row, $P_{i,\cdot}$, of P is an embedding dimension, which should assign similar values to the nearby landmarks on the manifolds. As we mentioned earlier, there are three localities to serve as similarities, where they behave similarly in this case. With either of the three, one can define the Optimization 1 or Optimization 2. In this simple case, the different similarity definitions are almost identical, leading to a spectral solution of P . Let's choose a simple construction [65]: given a data point $\vec{x} \in \mathbb{R}^2$, add Gaussian noise ϵ_1, ϵ_2 to it to generate two augmented samples $\vec{x}_1 = x_1 + \epsilon_1$ and $\vec{x}_2 = x_2 + \epsilon_2$, which are marked as the red and green crosses in Figure 2(b) and are considered as similar data points. $f(\vec{x}_1)$ and $f(\vec{x}_2)$ are marked as red and green dots (landmarks). So the objective in Optimization 1 is to find P such that $\mathbb{E}_{x \sim p(x), \epsilon_1, \epsilon_2 \sim \mathcal{N}(0, I)} \|Pf(x_1 + \epsilon_1) - Pf(x_2 + \epsilon_2)\|^2$ is minimized. We show the solution in Figure 2(c) with the first four embedding dimensions, $\{P_{1,\cdot}, P_{2,\cdot}, P_{3,\cdot}, P_{4,\cdot}\}$ plotted, where the color reflect their values at each dictionary element. As we can see, each embedding dimension, e.g. $P_{i,\cdot}$, is essentially a low-frequency function. $P_{1,\cdot}, P_{2,\cdot}$ are piecewise constant functions on the union of the manifolds. Essentially, either $P_{1,\cdot}$ or $P_{2,\cdot}$ will suffice to determine which manifold a point belongs to. $P_{2,\cdot}, P_{3,\cdot}$ are non-constant linear functions along the manifolds. A linear combination of $P_{3,\cdot}$ and $P_{4,\cdot}$ will preserve the coordinate information of the manifolds. Now with both the sparse feature function f and the spectral embedding P , we have constructed a sparse manifold transform, i.e. $\vec{\beta} = Pf(\vec{x})$. In Figure 2(d), we show how each dimension of this transform assigns different values to each point in the original 2D space, and the points from the same manifold are placed much closer in the representation space as shown in Figure 2(f).

³1-sparse sparse coding is equivalent to clustering. Sampling the data as the dictionary also suffices here.

Probabilistic point of view: co-occurrence modeling. Many related variations of spectral and matrix factorization methods have been widely used to build continuous word representations. SMT formulation bears a probabilistic point of view, which complements the manifold perspective. A notable example is the word co-occurrence problem. Here we present an SMT-word embedding. Given a corpus and a token dictionary, we can treat each token as a 1-hot vector $\vec{\alpha}$. Then we can seek a linear projection P such that tokens co-occur within a certain size context window are linearly projected closer. After we solve Optimization 1, each column of P corresponds to a continuous embedding of an element from the token dictionary. We train SMT on WikiText-103 [70] and provide the visualization result in Appendix A. As we discussed earlier, “Seattle” and “Dallas” may reach a similar embedding though they do not co-occur the most frequently. The probabilistic view of SMT explains the phenomenon that two embedding vectors can be close in the representation space if they frequently appear in similar contexts, though they may not be close in the signal space.

Sparsity, locality, compositionality, and hierarchy. (a) Sparsity: In the sparse manifold transform, sparsity mainly captures the locality and compositionality, which builds a support for the spectral embedding. Spectral embedding, on the other hand, would assign similar values to similar points on the support. (b) Locality: In a low-dimensional space, e.g., the 2D manifold disentanglement case, with enough landmarks, using 1-sparse feature f_{vq} to capture locality will suffice, and SMT can directly solve the problem as we showed earlier. Please note that, in this simple case, this process is not different from manifold learning [82; 96] and spectral clustering [74]. One can also use a kernel, e.g. RBF kernel or the heat kernel, to respect locality by lifting to a higher or infinite dimensional space [87; 102; 5; 94; 7]. (c) Compositionality: If the signal comes from a high-dimensional space, e.g. images, then we may need to build the representation for image patches first since even local neighborhoods can become less reliable in high-dimensional space with finite samples. If the patch space is simple enough, e.g. MNIST, using 1-sparse vector quantization as the sparse feature f_{vq} would be sufficient to capture the locality in patch space. As we will show later in Section 3, the SMT with 1-sparse feature f_{vq} achieves over 99.3% top-1 KNN accuracy. For more complex natural images, e.g. CIFAR or ImageNet, compositionality exists even in the patch space. So 1-sparse feature becomes less efficient and may compromise the fidelity of the representation. As we will show, the general sparse feature will achieve better performance than the 1-sparse feature in this case. (d) Hierarchy: For high-resolution images, we may need to stack several layers of transforms in order to handle the hierarchical representation [99; 33; 49].

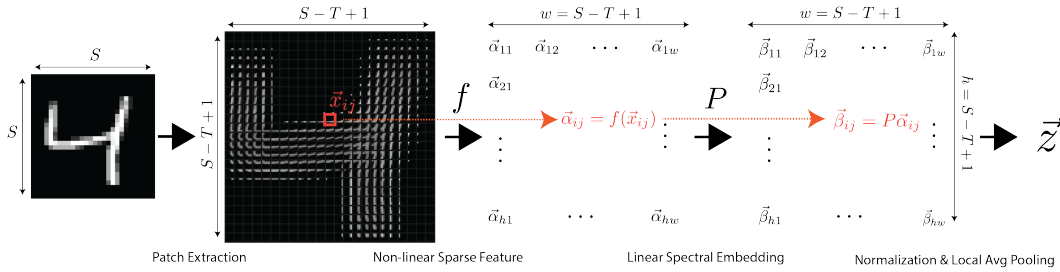


Figure 3: SMT representation of an image and its patches. An $S \times S$ image is first decomposed into $(S - T + 1) \times (S - T + 1)$ overlapping image patches of size $T \times T$. Each image patch is whitened and the sparse feature is calculated, $\vec{\alpha}_{ij} = f(\vec{x}_{ij})$, where ij indicates the spatial index of the image patch and \vec{x}_{ij} is the whitened patch. The representation of patch \vec{x}_{ij} is $\vec{\beta}_{ij} = P f(\vec{x}_{ij})$ with a L2 normalization. If we denote all of the patch representations from an image as tensor B , the image representation is $\vec{z} = \text{L2_normalize_pw}(\text{avg_pool}(B; \text{ks}, \text{stride}))$. $\text{avg_pool}(\cdot; \text{ks}, \text{stride})$ denotes the average pooling operator, where ks and stride are the kernel size and stride size respectively. L2_normalize_pw denotes a point-wise L2 normalization. We use tensor \vec{z} as a vector for an image representation. For MNIST experiments, we choose the patch embedding dimension as 32 by default. For CIFAR experiments, we choose the patch embedding dimension as 384 by default.

SMT representation for MNIST and CIFAR. We use SMT to build representation for image patches and aggregate patch representation of an image as the image representation. For an $S \times S$ image, we extract every $T \times T$ image patches as shown in Figure 3. Each of the image patches is whitened and L2-normalized. Given an image, we denote the pre-processed image patches as

$\{\vec{x}_{ij}\}$, where i indicates the vertical index of the patch and j indicates the horizontal index. For each image patch $\{\vec{x}_{ij}\}$, we define its neighbors to be other patches within a certain pixel range from it on the same image, i.e., $n(ij) = \{lm; |i-l| \leq d \text{ and } |j-m| \leq d\}$. Given a sparse feature function f , we would like to map these neighboring patches to be close in the representation space. If we choose $d = S - T + 1$, then all the patches from the same image are treated as neighbors to each other. Given f , d , and a set of training images, we can calculate $ADD^T A^T$, V , and solve Optimization 1 for P^4 . The representation of patch \vec{x}_{ij} is $\vec{\beta}_{ij} = Pf(\vec{x}_{ij})$ with a L2 normalization. If we denote all of the patch representations from an image as tensor B , the image representation is $\vec{z} = \text{L2_normalize_pw}(\text{avg_pool}(B; \text{ks}, \text{stride}))$. $\text{avg_pool}(\cdot; \text{ks}, \text{stride})$ denotes the average pooling operator, where ks and stride are the kernel size and stride size respectively. L2_normalize_pw denotes a point-wise L2 normalization. We use tensor \vec{z} as a vector for an image representation. The detailed settings, e.g. d , ks , stride , etc., are left to the experiments section. In this work, we primarily use the soft-KNN classifier to evaluate the quality of representation.

Connection to the deep latent-embedding methods. There are important connection between the SOTA latent-embedding SSL methods[17; 4]. In particular, Optimization 1 can be considered the simplest form of VICReg [4], whereas the VC regularization is replaced by a hard constraint, and a sparse feature function replaces the deep neural encoder. This connection is even stronger given the evidence that VICReg is essentially building a representation of image patches [21]. In this sense, SMT can be considered the simplest form of VICReg.

3 EMPIRICAL RESULTS

In this section, we first provide the benchmark results on MNIST, CIFAR10, and CIFAR100. Qualitative visualization is also provided for a better understanding. We also compare 1-sparse feature f_{vq} and a more general sparse feature f_{gq} . $\vec{\alpha} = f_{vq}(\vec{x}; D)$ refers to the 1-sparse vector quantization sparse feature, where $\alpha_i = 1$ for $i = \text{argmax}_i \|\vec{x} - D_{\cdot,i}\|_2$ and D is a dictionary. We denote the SMT representation with f_{vq} sparse feature as SMT-VQ. $\vec{\alpha} = f_{gq}(\vec{x}; D, t)$ refers to a more general sparse function, where each column of dictionary D is an image patch and t is a given threshold. For $\vec{\alpha} = f_{gq}(\vec{x}; D, t)$, the i th entry of $\vec{\alpha}$ is 1 only if the cosine similarity between \vec{x} and i th dictionary element pass the threshold, i.e., $\alpha_i = 1$ if $\cos(\vec{x}, D_{\cdot,i}) \geq t$ and $\alpha_i = 0$ otherwise. We denote the SMT representation with f_{gq} feature as SMT-GQ. We find f_{gq} achieves similar performance as the sparse coding feature in benchmarks, and it's more efficient in experiments since it does not involve a loopy inference. For both MNIST and CIFAR, we use 6x6 image patches, i.e., $T = 6$. All the image patches are whitened, and the whitening transform is described in Appendix C.

Table 1: **Evaluation of SMT representation on MNIST.** The table shows the evaluation result of SMT embedding and GloVe embedding on MNIST dataset using KNN classifiers. We compare different dictionary size, 16384 and 65536, context range, 3-Pixel ($d = 3$) and Whole Image ($d = 28 - 6 + 1$). We use 32 as the embedding dimension. As shown in the table, GloVe embedding works slightly worse than SMT embedding.

Co-Occurrence Context Range	SMT-VQ (16384)	SMT-VQ (65536)	SMT-VQ (GloVe, 100K)
Whole Image	99.0%	98.9%	98.8%
3 Pixels	99.2%	99.3%	99.0%

MNIST. As we mentioned earlier, once we decompose the MNIST image into patches, 1-sparse feature f_{vq} is sufficient to build a good support of the patch space. The dictionary $D \in \mathbb{R}^{36 \times K}$ is learned through 1-sparse sparse coding, which is equivalent to a clustering process with a GPU implementation. The detailed learning procedure is left to Appendix D. The inference is equivalent to vector quantization. In Table 1, we compare different dictionary sizes and different spatial co-occurrence range. The dimension of the embeddings is 32 dimensional, where further increasing the dimension does not improve the performance. Treating each image patch as a token and the entire image patches as sentences, we can also train a GloVe word embedding model on MNIST patches. We provide a GloVe embedding with optimized settings. As we can see in Table 1, GloVe embedding works slightly worse in this case, even with a large dictionary size. Further, we can find

⁴While a SGD algorithm can be used[20], we use deterministic algorithm in this paper.

that a small context range works slightly better for MNIST. This is probably due to that the patch space of MNIST is closer to a manifold, and co-occurrence is less informative in this case. To further verify this hypothesis, we provide an ablation study on embedding dimensions in Table 2. Even if we reduce the embedding dimension to 4⁵, the top-1 KNN accuracy is still 98.8%. This implies that the MNIST patch space might be close to a manifold like high-contrast natural image patches [63; 24; 11].

Table 2: **Low dimensionality of MNIST patch space.** The table shows the effect of the embedding dimension of SMT on the KNN evaluation accuracy. Even with 4-dimensional embedding for each patch, the KNN accuracy can still achieve 98.8%, which shows that the MNIST patch space can be viewed as a 3-manifold (it is on a hypersphere).

	Emb Dim=2	Emb Dim=3	Emb Dim=4	Emb Dim=8	Emb Dim=16	Emb Dim=32
KNN Acc	97.1%	98.3%	98.8%	99.0%	99.1%	99.2%

CIFAR10 and CIFAR100. For the CIFAR benchmarks, we compare both $f_{vq}(\cdot; D)$ and $f_{gq}(\cdot; D, t)$. The dictionary D used in f_{vq} is learned through 1-sparse sparse coding, and the dictionary D used in f_{gq} is just randomly sampled from all image patches for efficiency purposes. First, with gray-scale patches, we find that f_{vq} and f_{gq} work equally well. However, since f_{vq} with color patches underperforms that with gray-scale patches, we choose to experiment mostly with f_{gq} on CIFAR benchmarks. For f_{gq} , t is set to 0.3 with color patches and 0.45 with gray-scale patches. For CIFAR experiments, we choose the patch embedding dimension as 384 by default. Further, with color patches, dropping the first 16 embedding dimensions of P improves the accuracy by about 1%. SMT training uses both the original training set and the horizontally flipped version. On the other hand, SSL models use image flip augmentation as their default setting. For the “Original + Gray Scale” augmentation, SMT-GQ simply concatenates the embedding of color patch embedding and the gray-scale patch embedding. With a two-layer deterministic construction using only image patches, SMT significantly outperforms the SOTA methods, SimCLR and VICReg, with no color augmentation. Please note that SimCLR and VICReg still use random-resized crop augmentation. With grayscale-only color augmentation, SMT-GQ achieves similar performance as SimCLR and VICReg. SMT-GQ with “+gray scale” augmentation performs on par with SimCLR and VICReg without colorjitter and several additional color augmentations. SimCLR and VICReg, with full data augmentation, outperform SMT-GQ. However, we did not find a straightforward way to add these color augmentations to SMT-GQ. We can observe the same trend on CIFAR100. Interestingly, SMT-GQ always significantly outperforms SimCLR and VICReg before we add color jittering and additional data augmentations. We provide further ablation study in Appendix E to show two components of sparse manifold transforms: sparse feature and spectral embedding are both crucial for building good representations. Only if we use spectral embedding, will the performance scale with a larger dictionary. The performance of SMT will significantly degrade if we replace spectral embedding with some other dimension reduction algorithm that doesn’t respect locality.

Table 3: **Evaluation of SMT and SSL pretrained model on CIFAR10.** The table shows the evaluation result of SMT embedding and SSL pretrained models using KNN classifiers. We evaluated various color augmentation schemes. For “original image”, we use only “horizontal flip” data augmentation for SMT, and use both “horizontal flip” and “random resized crop” data augmentation for SSL methods. For “Full”, we added both “grayscale” and “colorjitter” color augmentation on top of other data augmentations in “original image”. We tried two sparse feature for SMT: f_{vq} and f_{gq} . For f_{gq} , we tried two dictionary sizes: 8192 and 65536. Both SSL models uses ResNet-18 as backbone and is optimized for 1000 epochs through propagation; SMT uses a 2-layer architecture and is analytically solved.

Color Augmentation	SMT-VQ (100K)	SMT-GQ (8192)	SMT-GQ (65536)	SimCLR (ResNet18)	VICReg (ResNet18)
Original Image	—	79.2%	81.1%	68.3%	70.2%
Grayscale Image Only	78.4%	77.5%	78.9%	80.6%	81.3%
Original + Grayscale	—	81.4%	83.2%	85.7%	83.7%
Full (ColorJitter etc.)	—	—	—	90.1%	91.1%

⁵As the embedding is further L2 normalized, this is a 3-dimensional space.

Table 4: **Evaluation of SMT and SSL pretrained model on CIFAR100.** The table shows the performance of SMT embedding and two other SSL pretraining methods on the CIFAR100 dataset. The data augmentation and different SMT variations we used in this experiment is the same as those for evaluating CIFAR10 dataset in Table 3. For CIFAR100 dataset, without full color augmentation, SMT always outperforms the two SSL pretraining methods.

Color Augmentation	SMT-VQ (100K)	SMT-GQ (8192)	SMT-GQ (65536)	SimCLR (ResNet18)	VICReg (ResNet18)
Original Image	—	50.8%	53.2%	32.4%	32.6%
Grayscale Image	46.6%	45.8%	48.9%	43.0%	43.9%
Original + Grayscale	—	53.7%	57.0%	48.9%	46.0%
Full (ColorJitter etc.)	—	—	—	63.7%	65.4%

Visualization. For a better understanding, we provide a visualization of the patch embedding space with the 1-sparse feature in Figure 4. Given a dictionary D , each dictionary element is an image patch in the whitened space. For a dictionary element shown in the red box, we can visualize its nearest neighbors, measured by cosine similarity, in the embedding space. All the image patches are unwhitened before visualization, where the detail is left to the Appendix C. In Figure 4, we can see that the nearest neighbors are all semantically similar. a) is a slightly curved stroke of a digit in MNIST. b) shows the patch of the center of a digit “4”. c) shows a part of a “wheel” of a car in CIFAR. d) shows a part of “animal face”. These results are similar to the 2D results shown in Figure 2. The sparse feature respects the locality in the data space and provides a support for the representation transform and spectral embedding, assigning similar values to similar points on the support. Overall the representation transform brings similar points in the data space closer in the representation space.

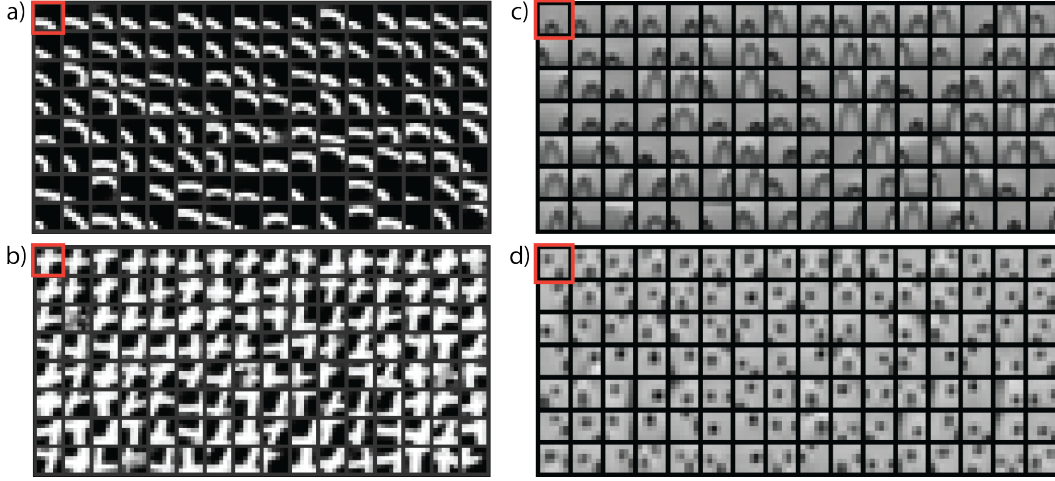


Figure 4: **Visualization of dictionary elements’ neighborhoods in the SMT embedding space.** We plot 4 different dictionary element and their top nearest neighbors in four subfigures, respectively. For each subfigure, the dictionary element is shown in the red box. Its neighboring patches in the representation space are ordered by their cosine similarity to the dictionary element, where the image patches in the top left have highest cosine similarity, and image patches on the bottom right have lowest cosine similarity. This figure is qualitatively similar to Figure 2(f) except it is in a high-dimensional space and the semantic meaning is more complex.

4 MORE RELATED WORKS

There are several intertwined quests closely related to this work. Here, we touch them briefly.

The state-of-the-art unsupervised methods. Deep learning [59; 62] is the engine behind the recent revolution of AI. Given the right craftsmanship, deep neural networks are powerful optimization tools to allow us express various engineering objectives conveniently. It has also revolutionized the unsupervised visual representation learning in the past few years [103; 45; 17; 4]. Understanding the

engineering advancements can help us gain deeper theoretical insights and many efforts have been made [66; 1] towards this goal.

To model the patterns of the signal spaces. A central challenge of modeling the signals is the formalization of a small set of ideas for constructing the representations of the patterns[41; 73]. Wavelet transform[67; 23] was formulated to handle the sparsity in the natural signals. Steerable and shiftable filters[36; 93; 91] were introduced to handle the discontinuity of wavelet filters with respect to the natural transformations. Basis pursuit[16; 15] finds decomposition of a signal by a predefined dictionary, sparse coding[75; 76], and ICA[6; 53] were proposed to learn the filters or dictionary from data. Before the sparse manifold transform[20], many important works have paved the way and introduced topology and transformations between the dictionary elements[54; 55; 10]. There are also several important works on studying the natural image patch space with non-parametric methods and topological tools [63; 24; 11; 46]. Manifold learning[82; 96; 42] and spectral clustering [31; 35; 87; 69; 74; 95; 86] was proposed to model the geometric structure in the signal space. The geometric signal process is also an increasingly important topic in signal processing [88].

Modeling of biological visual system. Exploring the geometric or statistical structure of natural signals are also strongly motivated by computational modeling of biological visual system. Many properties of the visual system reflect the structure of natural images [92; 56]. An early success of this quest was that the dictionary elements learned in an unsupervised fashion closely resemble the receptive fields of simple cells in the V1 cortex[75; 76]. In order to further understand the visual cortex, we need to develop theories that can help to elucidate how the cortex performs the computationally challenging problems of vision [77]. One important proposal is that the visual cortex performs hierarchical manifold disentanglement [29; 30]. The sparse manifold transform was formulated to solve this problem, which is supported by a recent perceptual evidence [47]. There are also several related seminal works on video linearization [102; 39; 38].

To build representation models from the first principles. The now classical models before deep learning use to be relatively simpler [60; 99; 80; 57; 101; 105], where sparsity was a widely adopted principle. While the gap between the SOTA deep learning model and the simple models is large, it might be smaller than many expect [22; 81; 9; 97]. The quest to build “white-box” models from the first principles [13; 12] for unsupervised representation remains an attractive open problem.

5 DISCUSSION

In this paper, we utilize two classical unsupervised learning principles, sparsity and spectral embedding, to build a minimalistic unsupervised representation with the sparse manifold transform [20]. The constructed “white-box” model achieves non-trivial performance on several benchmarks. Along the way, we address several fundamental questions and provide two complementary points of view, manifold disentanglement and co-occurrence modeling, of the proposed model. Further, the proposed method has close connections to VICReg [4] and several other SOTA latent-embedding SSL models [17; 107; 37]. There are several limits of this work, which point out the future directions: 1) We need to scale the method to larger datasets, e.g. ImageNet. 2) While a two-layer network achieves non-trivial performance, we need to further construct “white-box” hierarchical models to understand how a hierarchical representation is formed [48; 50]. 3) While spectral embedding is context-independent [79; 108], there is clear benefit in building contextualized embedding [27; 84; 49; 34; 106; 68]. It is an attractive topic to build minimalistic unsupervised representation based on contextualized embedding.

The evidence shows that it is a promising direction to build minimalistic “white-box” unsupervised learning models. Further reducing the gap and understanding why can lead us towards a theory. Minimalistic engineering models are easier to analyze and help us build a theory to identify optimality and efficiency. On the other hand, a testable theory can also facilitate the modeling of biological learning systems. This work makes a step towards this goal.

ACKNOWLEDGMENTS

We thank Fritz Sommer, Zengyi Li, John Wright, Jiachen Zhu, Quentin Garrido, Randall Balestriero, Bobak Kiani, Christopher Kymn, Jamie Simon, Sam Buchanan, Jiayun Wang and many other colleagues for their helpful comments and inspiring discussions.

REFERENCES

- [1] Sanjeev Arora, Simon S Du, Wei Hu, Zhiyuan Li, Russ R Salakhutdinov, and Ruosong Wang. On exact computation with an infinitely wide neural net. *Advances in Neural Information Processing Systems*, 32, 2019.
- [2] Sanjeev Arora, Hrishikesh Khandeparkar, Mikhail Khodak, Orestis Plevrakis, and Nikunj Saunshi. A theoretical analysis of contrastive unsupervised representation learning. *arXiv preprint arXiv:1902.09229*, 2019.
- [3] Randall Balestriero and Yann LeCun. Contrastive and non-contrastive self-supervised learning recover global and local spectral embedding methods. *arXiv preprint arXiv:2205.11508*, 2022.
- [4] Adrien Bardes, Jean Ponce, and Yann LeCun. Vicreg: Variance-invariance-covariance regularization for self-supervised learning. *arXiv preprint arXiv:2105.04906*, 2021.
- [5] Mikhail Belkin and Partha Niyogi. Laplacian eigenmaps for dimensionality reduction and data representation. *Neural computation*, 15(6):1373–1396, 2003.
- [6] Anthony J Bell and Terrence J Sejnowski. An information-maximization approach to blind separation and blind deconvolution. *Neural computation*, 7(6):1129–1159, 1995.
- [7] Yoshua Bengio, Aaron Courville, and Pascal Vincent. Representation learning: A review and new perspectives. *IEEE transactions on pattern analysis and machine intelligence*, 35(8):1798–1828, 2013.
- [8] Florian Bordes, Randall Balestriero, and Pascal Vincent. High fidelity visualization of what your self-supervised representation knows about. *arXiv preprint arXiv:2112.09164*, 2021.
- [9] Wieland Brendel and Matthias Bethge. Approximating cnns with bag-of-local-features models works surprisingly well on imagenet. *arXiv preprint arXiv:1904.00760*, 2019.
- [10] Charles F Cadieu and Bruno A Olshausen. Learning intermediate-level representations of form and motion from natural movies. *Neural computation*, 24(4):827–866, 2012.
- [11] Gunnar Carlsson, Tigran Ishkhanov, Vin De Silva, and Afra Zomorodian. On the local behavior of spaces of natural images. *International journal of computer vision*, 76(1):1–12, 2008.
- [12] Kwan Ho Ryan Chan, YD Yu, Chong You, Haozhi Qi, John Wright, and Yi Ma. Redunet: A white-box deep network from the principle of maximizing rate reduction. *J Mach Learn Res*, 23(114):1–103, 2022.
- [13] Tsung-Han Chan, Kui Jia, Shenghua Gao, Jiwen Lu, Zinan Zeng, and Yi Ma. Pcanet: A simple deep learning baseline for image classification? *IEEE transactions on image processing*, 24(12):5017–5032, 2015.
- [14] Hila Chefer, Shir Gur, and Lior Wolf. Generic attention-model explainability for interpreting bi-modal and encoder-decoder transformers. In *Proceedings of the IEEE/CVF International Conference on Computer Vision*, pp. 397–406, 2021.
- [15] Scott Shaobing Chen, David L Donoho, and Michael A Saunders. Atomic decomposition by basis pursuit. *SIAM review*, 43(1):129–159, 2001.
- [16] Shaobing Chen and David Donoho. Basis pursuit. In *Proceedings of 1994 28th Asilomar Conference on Signals, Systems and Computers*, volume 1, pp. 41–44. IEEE, 1994.
- [17] Ting Chen, Simon Kornblith, Mohammad Norouzi, and Geoffrey Hinton. A simple framework for contrastive learning of visual representations. In *International conference on machine learning*, pp. 1597–1607. PMLR, 2020.
- [18] Xinlei Chen and Kaiming He. Exploring simple siamese representation learning. In *Proceedings of the IEEE/CVF Conference on Computer Vision and Pattern Recognition*, pp. 15750–15758, 2021.

- [19] Xinlei Chen, Haoqi Fan, Ross Girshick, and Kaiming He. Improved baselines with momentum contrastive learning. *arXiv preprint arXiv:2003.04297*, 2020.
- [20] Yubei Chen, Dylan M. Paiton, and Bruno A. Olshausen. The sparse manifold transform. In *Advances in Neural Information Processing Systems 31: Annual Conference on Neural Information Processing Systems 2018, NeurIPS 2018, December 3-8, 2018, Montréal, Canada*, pp. 10534–10545, 2018.
- [21] Yubei Chen, Adrien Bardes, Zengyi Li, and Yann LeCun. Intra-instance vicreg: Bag of self-supervised image patch embedding. *arXiv preprint arXiv:2206.08954*, 2022.
- [22] Adam Coates, Andrew Ng, and Honglak Lee. An analysis of single-layer networks in unsupervised feature learning. In *Proceedings of the fourteenth international conference on artificial intelligence and statistics*, pp. 215–223. JMLR Workshop and Conference Proceedings, 2011.
- [23] Ingrid Daubechies. Orthonormal bases of compactly supported wavelets. *Communications on pure and applied mathematics*, 41(7):909–996, 1988.
- [24] Vin De Silva and Gunnar E Carlsson. Topological estimation using witness complexes. *SPBG*, 4:157–166, 2004.
- [25] Vin De Silva and Joshua B Tenenbaum. Sparse multidimensional scaling using landmark points. Technical report, Technical report, Stanford University, 2004.
- [26] Scott Deerwester, Susan T Dumais, George W Furnas, Thomas K Landauer, and Richard Harshman. Indexing by latent semantic analysis. *Journal of the American society for information science*, 41(6):391–407, 1990.
- [27] Jacob Devlin, Ming-Wei Chang, Kenton Lee, and Kristina Toutanova. Bert: Pre-training of deep bidirectional transformers for language understanding. *arXiv preprint arXiv:1810.04805*, 2018.
- [28] Inderjit S. Dhillon and Dharmendra S. Modha. Concept decompositions for large sparse text data using clustering. *Machine Learning*, 42(1):143–175, 2001.
- [29] James J DiCarlo and David D Cox. Untangling invariant object recognition. *Trends in cognitive sciences*, 11(8):333–341, 2007.
- [30] James J DiCarlo, Davide Zoccolan, and Nicole C Rust. How does the brain solve visual object recognition? *Neuron*, 73(3):415–434, 2012.
- [31] William E Donath and Alan J Hoffman. Lower bounds for the partitioning of graphs. In *Selected Papers Of Alan J Hoffman: With Commentary*, pp. 437–442. World Scientific, 2003.
- [32] Susan T Dumais. Latent semantic analysis. *Annual Review of Information Science and Technology (ARIST)*, 38:189–230, 2004.
- [33] Boris Epshtein and Shimon Ullman. Semantic hierarchies for recognizing objects and parts. In *2007 IEEE Conference on Computer Vision and Pattern Recognition*, pp. 1–8. IEEE, 2007.
- [34] Kawin Ethayarajh. How contextual are contextualized word representations? comparing the geometry of bert, elmo, and gpt-2 embeddings. *arXiv preprint arXiv:1909.00512*, 2019.
- [35] Miroslav Fiedler. Algebraic connectivity of graphs. *Czechoslovak mathematical journal*, 23(2):298–305, 1973.
- [36] William T Freeman, Edward H Adelson, et al. The design and use of steerable filters. *IEEE Transactions on Pattern analysis and machine intelligence*, 13(9):891–906, 1991.
- [37] Quentin Garrido, Yubei Chen, Adrien Bardes, Laurent Najman, and Yann Lecun. On the duality between contrastive and non-contrastive self-supervised learning. *arXiv preprint arXiv:2206.02574*, 2022.

- [38] Ross Goroshin, Joan Bruna, Jonathan Tompson, David Eigen, and Yann LeCun. Unsupervised learning of spatiotemporally coherent metrics. In *Proceedings of the IEEE international conference on computer vision*, pp. 4086–4093, 2015.
- [39] Ross Goroshin, Michael F Mathieu, and Yann LeCun. Learning to linearize under uncertainty. *Advances in neural information processing systems*, 28, 2015.
- [40] Robert M. Gray. Vector quantization. *IEEE ASSP Magazine*, 1:4–29, 1984.
- [41] Ulf Grenander and Michael I Miller. *Pattern theory: from representation to inference*. OUP Oxford, 2006.
- [42] Raia Hadsell, Sumit Chopra, and Yann LeCun. Dimensionality reduction by learning an invariant mapping. In *2006 IEEE Computer Society Conference on Computer Vision and Pattern Recognition (CVPR’06)*, volume 2, pp. 1735–1742. IEEE, 2006.
- [43] Jeff Z HaoChen, Colin Wei, Adrien Gaidon, and Tengyu Ma. Provable guarantees for self-supervised deep learning with spectral contrastive loss. *Advances in Neural Information Processing Systems*, 34:5000–5011, 2021.
- [44] Tatsunori B Hashimoto, David Alvarez-Melis, and Tommi S Jaakkola. Word, graph and manifold embedding from markov processes. *arXiv preprint arXiv:1509.05808*, 2015.
- [45] Kaiming He, Haoqi Fan, Yuxin Wu, Saining Xie, and Ross Girshick. Momentum contrast for unsupervised visual representation learning. In *Proceedings of the IEEE/CVF conference on computer vision and pattern recognition*, pp. 9729–9738, 2020.
- [46] Olivier J. Hénaff, Johannes Ballé, Neil C. Rabinowitz, and Eero P. Simoncelli. The local low-dimensionality of natural images. In *3rd International Conference on Learning Representations, ICLR 2015, San Diego, CA, USA, May 7-9, 2015, Conference Track Proceedings*, 2015.
- [47] Olivier J Hénaff, Robbe LT Goris, and Eero P Simoncelli. Perceptual straightening of natural videos. *Nature neuroscience*, 22(6):984–991, 2019.
- [48] Geoffrey Hinton. Some demonstrations of the effects of structural descriptions in mental imagery. *Cognitive Science*, 3(3):231–250, 1979.
- [49] Geoffrey Hinton. How to represent part-whole hierarchies in a neural network. *arXiv preprint arXiv:2102.12627*, 2021.
- [50] Geoffrey E Hinton. Mapping part-whole hierarchies into connectionist networks. *Artificial Intelligence*, 46(1-2):47–75, 1990.
- [51] Geoffrey E Hinton and Sam Roweis. Stochastic neighbor embedding. *Advances in neural information processing systems*, 15, 2002.
- [52] Junqiang Huang, Xiangwen Kong, and Xiangyu Zhang. Revisiting the critical factors of augmentation-invariant representation learning. *arXiv preprint arXiv:2208.00275*, 2022.
- [53] Aapo Hyvärinen and Erkki Oja. A fast fixed-point algorithm for independent component analysis. *Neural computation*, 9(7):1483–1492, 1997.
- [54] Aapo Hyvärinen, Patrik O Hoyer, and Mika Inki. Topographic independent component analysis. *Neural computation*, 13(7):1527–1558, 2001.
- [55] Aapo Hyvärinen, Jarmo Hurri, and Jaakko Väyrynen. Bubbles: a unifying framework for low-level statistical properties of natural image sequences. *JOSA A*, 20(7):1237–1252, 2003.
- [56] Aapo Hyvärinen, Jarmo Hurri, and Patrick O Hoyer. *Natural image statistics: A probabilistic approach to early computational vision.*, volume 39. Springer Science & Business Media, 2009.

- [57] Herve Jegou, Matthijs Douze, and Cordelia Schmid. Product quantization for nearest neighbor search. *IEEE transactions on pattern analysis and machine intelligence*, 33(1):117–128, 2010.
- [58] Li Jing, Jiachen Zhu, and Yann LeCun. Masked siamese convnets. *arXiv preprint arXiv:2206.07700*, 2022.
- [59] Alex Krizhevsky, Ilya Sutskever, and Geoffrey E Hinton. Imagenet classification with deep convolutional neural networks. *Communications of the ACM*, 60(6):84–90, 2017.
- [60] Svetlana Lazebnik, Cordelia Schmid, and Jean Ponce. Beyond bags of features: Spatial pyramid matching for recognizing natural scene categories. In *2006 IEEE computer society conference on computer vision and pattern recognition (CVPR’06)*, volume 2, pp. 2169–2178. IEEE, 2006.
- [61] Y LeCun. A path towards autonomous machine intelligence. *preprint posted on openreview*, 2022.
- [62] Yann LeCun, Yoshua Bengio, and Geoffrey Hinton. Deep learning. *nature*, 521(7553):436–444, 2015.
- [63] Ann B Lee, Kim S Pedersen, and David Mumford. The nonlinear statistics of high-contrast patches in natural images. *International Journal of Computer Vision*, 54(1):83–103, 2003.
- [64] Omer Levy and Yoav Goldberg. Linguistic regularities in sparse and explicit word representations. In *Proceedings of the eighteenth conference on computational natural language learning*, pp. 171–180, 2014.
- [65] Zengyi Li, Yubei Chen, Yann LeCun, and Friedrich T Sommer. Neural manifold clustering and embedding. *arXiv preprint arXiv:2201.10000*, 2022.
- [66] Zhiyuan Li, Ruosong Wang, Dingli Yu, Simon S Du, Wei Hu, Ruslan Salakhutdinov, and Sanjeev Arora. Enhanced convolutional neural tangent kernels. *arXiv preprint arXiv:1911.00809*, 2019.
- [67] Stephane G Mallat. A theory for multiresolution signal decomposition: the wavelet representation. *IEEE transactions on pattern analysis and machine intelligence*, 11(7):674–693, 1989.
- [68] Christopher D. Manning. Human Language Understanding & Reasoning. *Daedalus*, 151(2): 127–138, 05 2022.
- [69] Marina Meilă and Jianbo Shi. A random walks view of spectral segmentation. In *International Workshop on Artificial Intelligence and Statistics*, pp. 203–208. PMLR, 2001.
- [70] Stephen Merity, Caiming Xiong, James Bradbury, and Richard Socher. Pointer sentinel mixture models. In *5th International Conference on Learning Representations, ICLR 2017, Toulon, France, April 24-26, 2017, Conference Track Proceedings*. OpenReview.net, 2017.
- [71] Tomas Mikolov, Kai Chen, Greg Corrado, and Jeffrey Dean. Efficient estimation of word representations in vector space. *arXiv preprint arXiv:1301.3781*, 2013.
- [72] Tomas Mikolov, Ilya Sutskever, Kai Chen, Greg S Corrado, and Jeff Dean. Distributed representations of words and phrases and their compositionality. *Advances in neural information processing systems*, 26, 2013.
- [73] David Mumford and Agnès Desolneux. *Pattern theory: the stochastic analysis of real-world signals*. CRC Press, 2010.
- [74] Andrew Ng, Michael Jordan, and Yair Weiss. On spectral clustering: Analysis and an algorithm. *Advances in neural information processing systems*, 14, 2001.
- [75] Bruno A Olshausen and David J Field. Emergence of simple-cell receptive field properties by learning a sparse code for natural images. *Nature*, 381(6583):607, 1996.

- [76] Bruno A Olshausen and David J Field. Sparse coding with an overcomplete basis set: A strategy employed by v1? *Vision research*, 37(23):3311–3325, 1997.
- [77] Bruno A Olshausen and David J Field. How close are we to understanding v1? *Neural computation*, 17(8):1665–1699, 2005.
- [78] Aaron van den Oord, Yazhe Li, and Oriol Vinyals. Representation learning with contrastive predictive coding. *arXiv preprint arXiv:1807.03748*, 2018.
- [79] Jeffrey Pennington, Richard Socher, and Christopher D Manning. Glove: Global vectors for word representation. In *Proceedings of the 2014 conference on empirical methods in natural language processing (EMNLP)*, pp. 1532–1543, 2014.
- [80] Florent Perronnin, Jorge Sánchez, and Thomas Mensink. Improving the fisher kernel for large-scale image classification. In *European conference on computer vision*, pp. 143–156. Springer, 2010.
- [81] Benjamin Recht, Rebecca Roelofs, Ludwig Schmidt, and Vaishal Shankar. Do imagenet classifiers generalize to imagenet? In *International Conference on Machine Learning*, pp. 5389–5400. PMLR, 2019.
- [82] Sam T Roweis and Lawrence K Saul. Nonlinear dimensionality reduction by locally linear embedding. *science*, 290(5500):2323–2326, 2000.
- [83] David E Rumelhart, Geoffrey E Hinton, and Ronald J Williams. Learning representations by back-propagating errors. *nature*, 323(6088):533–536, 1986.
- [84] Justyna Sarzynska-Wawer, Aleksander Wawer, Aleksandra Pawlak, Julia Szymanowska, Izabela Stefaniak, Michal Jarkiewicz, and Lukasz Okruszek. Detecting formal thought disorder by deep contextualized word representations. *Psychiatry Research*, 304:114135, 2021.
- [85] Lawrence K Saul and Sam T Roweis. Think globally, fit locally: unsupervised learning of low dimensional manifolds. *Journal of machine learning research*, 4(Jun):119–155, 2003.
- [86] Geoffrey Schiebinger, Martin J Wainwright, and Bin Yu. The geometry of kernelized spectral clustering. *The Annals of Statistics*, 43(2):819–846, 2015.
- [87] Jianbo Shi and Jitendra Malik. Normalized cuts and image segmentation. *IEEE Transactions on pattern analysis and machine intelligence*, 22(8):888–905, 2000.
- [88] David I Shuman, Sunil K Narang, Pascal Frossard, Antonio Ortega, and Pierre Vandergheynst. The emerging field of signal processing on graphs: Extending high-dimensional data analysis to networks and other irregular domains. *IEEE signal processing magazine*, 30(3):83–98, 2013.
- [89] Ravid Shwartz-Ziv, Randall Balestriero, and Yann LeCun. What do we maximize in self-supervised learning? *arXiv preprint arXiv:2207.10081*, 2022.
- [90] Jorge Silva, Jorge Marques, and João Lemos. Selecting landmark points for sparse manifold learning. In *Advances in neural information processing systems*, pp. 1241–1248, 2006.
- [91] Eero P Simoncelli and William T Freeman. The steerable pyramid: A flexible architecture for multi-scale derivative computation. In *Proceedings., International Conference on Image Processing*, volume 3, pp. 444–447. IEEE, 1995.
- [92] Eero P Simoncelli and Bruno A Olshausen. Natural image statistics and neural representation. *Annual review of neuroscience*, 24(1):1193–1216, 2001.
- [93] Eero P Simoncelli, William T Freeman, Edward H Adelson, and David J Heeger. Shiftable multiscale transforms. *IEEE transactions on Information Theory*, 38(2):587–607, 1992.
- [94] Alex J Smola and Bernhard Schölkopf. A tutorial on support vector regression. *Statistics and computing*, 14(3):199–222, 2004.

- [95] X Yu Stella and Jianbo Shi. Multiclass spectral clustering. In *Computer Vision, IEEE International Conference on*, volume 2, pp. 313–313. IEEE Computer Society, 2003.
- [96] Joshua B Tenenbaum, Vin De Silva, and John C Langford. A global geometric framework for nonlinear dimensionality reduction. *science*, 290(5500):2319–2323, 2000.
- [97] Louis Thiry, Michael Arbel, Eugene Belilovsky, and Edouard Oyallon. The unreasonable effectiveness of patches in deep convolutional kernels methods. *arXiv preprint arXiv:2101.07528*, 2021.
- [98] Yuandong Tian, Xinlei Chen, and Surya Ganguli. Understanding self-supervised learning dynamics without contrastive pairs. In *International Conference on Machine Learning*, pp. 10268–10278. PMLR, 2021.
- [99] Shimon Ullman. Object recognition and segmentation by a fragment-based hierarchy. *Trends in cognitive sciences*, 11(2):58–64, 2007.
- [100] Max Vladymyrov and Miguel Á Carreira-Perpinán. Locally linear landmarks for large-scale manifold learning. In *Joint European Conference on Machine Learning and Knowledge Discovery in Databases*, pp. 256–271. Springer, 2013.
- [101] Jinjun Wang, Jianchao Yang, Kai Yu, Fengjun Lv, Thomas Huang, and Yihong Gong. Locality-constrained linear coding for image classification. In *2010 IEEE computer society conference on computer vision and pattern recognition*, pp. 3360–3367. IEEE, 2010.
- [102] Laurenz Wiskott and Terrence J Sejnowski. Slow feature analysis: Unsupervised learning of invariances. *Neural computation*, 14(4):715–770, 2002.
- [103] Zhirong Wu, Yuanjun Xiong, Stella X Yu, and Dahua Lin. Unsupervised feature learning via non-parametric instance discrimination. In *Proceedings of the IEEE conference on computer vision and pattern recognition*, pp. 3733–3742, 2018.
- [104] Chun-Hsiao Yeh, Cheng-Yao Hong, Yen-Chi Hsu, Tyng-Luh Liu, Yubei Chen, and Yann LeCun. Decoupled contrastive learning. *arXiv preprint arXiv:2110.06848*, 2021.
- [105] Kai Yu, Tong Zhang, and Yihong Gong. Nonlinear learning using local coordinate coding. *Advances in neural information processing systems*, 22, 2009.
- [106] Zeyu Yun, Yubei Chen, Bruno A Olshausen, and Yann LeCun. Transformer visualization via dictionary learning: contextualized embedding as a linear superposition of transformer factors. *arXiv preprint arXiv:2103.15949*, 2021.
- [107] Jure Zbontar, Li Jing, Ishan Misra, Yann LeCun, and Stéphane Deny. Barlow twins: Self-supervised learning via redundancy reduction. In *International Conference on Machine Learning*, pp. 12310–12320. PMLR, 2021.
- [108] Juexiao Zhang, Yubei Chen, Brian Cheung, and Bruno A Olshausen. Word embedding visualization via dictionary learning. *arXiv preprint arXiv:1910.03833*, 2019.

Appendix

A PROBABILISTIC POINT OF VIEW EXAMPLE: SMT WORD EMBEDDING

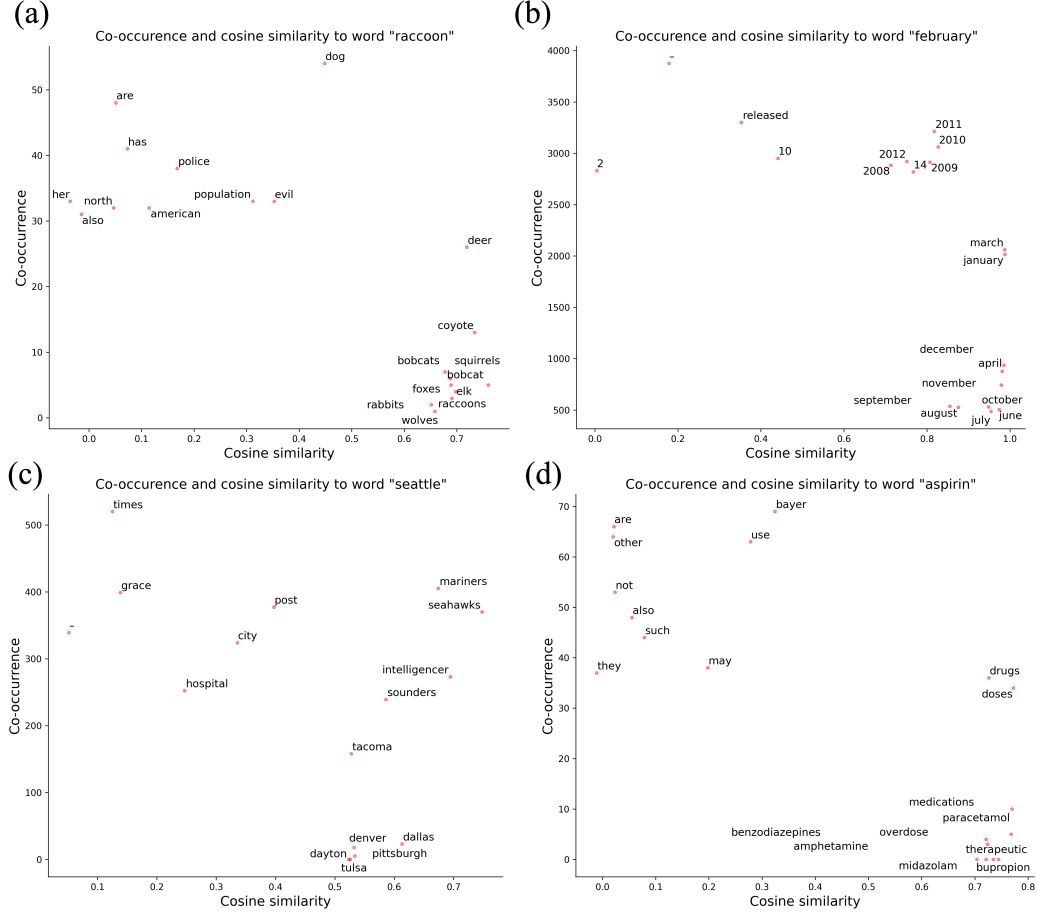


Figure 5: Visualization of SMT word embedding. For each word “raccoon”, “february”, “seattle” and “aspirin”, we plot the top 10 words that are closest to it in the embedding space, and we show the top 10 words that co-occur with it the most. Two words are close if the cosine similarity between their SMT embedding is high. The co-occurrence is calculated based on the entire corpus. We count two words that co-occurred once if they appear in the same context window. The co-occurrence is plotted against the cosine similarity.

We use SMT to build word embedding for the vocabulary in WikiText-103 to illustrate the probabilistic view of SMT. Unlike in Figure 2, where the neighbor of each data point x can be interpreted as its Euclidean neighborhood, there is no such distance function in the natural language. Nevertheless, we could still define neighborhood for each word. We define the neighbor of each word as other words that co-occur with it in a given context.

Like the manifold learning view, where the global geometry emerges despite only local neighborhoods being used during training, such a phenomenon is also observed from the probabilistic point of view. To visualize this phenomenon from a probabilistic point of view, we measure the co-occurrence of each pair of words and the cosine similarity between them in their SMT embedding space. In figure 5 (a), we show the top 10 words that are closest to “raccoon” and the top 10 words that co-occur the most with “raccoon”. We can see words like “American,” and “population” co-occur with “raccoon” a lot, but neither “American” nor “population” are close to “raccoon” in the embedding space. Instead, words that are semantically related to “raccoon” are close to “raccoon”

in the embedding space, like “squirrels”, “rabbits” and “wolves”, even though they rarely co-occur with “raccoon.” The underlying reason is that these words share the same context patterns as “raccoon”. Although words like “American” and “population” can co-occur with “raccoon” in phrases like “American raccoon” and “raccoon’s population,” these words also co-occur with other words in very different contexts. Thus, they could not be embedded to be close “raccoon.”

We also illustrate three more examples in figure 5. In (b), we see words that occur with “february” are other months like “july,” “june,” and “september.” In (c), words co-occur with “seattle” the most are other large cities like “dallas”, “denver” and “pittsburgh”, even though they rarely occur with “seattle.” Finally, in (d), the words co-occur with “aspirin” the most are names of other medicines.

B DETAILS FOR TRAINING WORD EMBEDDING USING SMT

Dataset. We use WikiText-103 corpus [70] to train SMT word embedding, which contains around 103 million tokens. For the tokenizer, we use “Basic English Tokenizer” from torchtext, which uses minimal text normalization. We tokenize and lowercase the WikiText-103 corpus, building a vocabulary using the top 33,474 words with the highest frequency. Notice that this dataset is significantly smaller than the Wikipedia dump used to train GLoVe in the original paper [79]. Wikipedia is also highly biased toward technical subjects, which is reflected in our word embedding.

SMT training. First, we choose the sparse extraction function f to be the one-hot encoding. Each token in the text corpus is considered a data point x_i ; it is first transformed into a one-hot vector by f , then encoded to be close to its neighbor via spectral embedding. In order to perform spectral embedding, we need to define the neighbor(context) for each word in Optimization 1. In this case, each word’s neighbor(context) is its previous eight words and the next eight words. We can then calculate $ADD^T A^T$, V , and solve Optimization 1 for P . The representation of each word in the vocabulary is simply each column of P . This is because f is one-hot encoding, for each word \vec{x}_i , we have $\vec{\beta}_i = Pf(\vec{x}_i) = P\mathbf{e}_i = \vec{P}_i$.

C WHITENING OF THE IMAGE PATCHES

We consider all the square image patches with size $T \times T \times c$, where T is patch size, and c is channel size, as flattened vectors of dimension T^2c . We first remove the mean from each patch. Instead of calculating the global mean like in the normal whitening procedure, we calculate the contextual mean. Let x_i denote a image patch and let $N_i = \{x_j : j \in n(i)\}$ denote the neighboring patch for x_i . We can calculate the contextual mean of x_i as $\mu_i = \frac{1}{|N_i|} \sum_{j \in N_i} x_j$. Let \bar{x}_i denote the mean removed image patch, then $\bar{x}_i = x_i - \mu_i$. We could also simply calculate the global mean μ and use it to center all the image patches. However, we found using contextual mean improve performance.

We apply the whitening operator to the mean-removed image patches. Let $\{\bar{x}_i\}$ denote the pre-processed image patches. Then we have

$$\vec{x}_i = (\lambda I + \Sigma)^{-\frac{1}{2}} \bar{x}_i$$

To “unwhiten” the patch for visualization, we multiply the whitened patch with the inverse of whiten operator: $(\lambda I + \Sigma)^{\frac{1}{2}}$.

D 1-SPARSE DICTIONARY LEARNING

Given $\vec{x}_i \in \mathbb{R}^d$ to be a data vector, and dictionary(codebook) $\Phi \in \mathbb{R}^{d \times K}$, where d is the dimension of the data and K is the number of dictionary elements, 1-Sparse Dictionary Learning, also known as Vector Quantization (VQ problem [40], can be formulated as:

$$\begin{aligned} \min_{\alpha_i, \Phi} \sum_i \|\vec{x}_i - \Phi \vec{\alpha}_i\|_2, \\ s.t. \quad \|\vec{\alpha}_i\|_0 = 1, \|\vec{\alpha}_i\|_1 = 1, \vec{\alpha}_i \succeq 0. \end{aligned} \tag{4}$$

This is an NP-hard problem, but there are efficient heuristic algorithms to approximate the solution. The most well-known one is K-mean clustering, which can be interpreted as an expectation-maximization (EM) algorithm for mixtures of Gaussian distributions. This is the algorithm we used

to solve 1-sparse dictionary learning when we use the 1-sparse feature f_{vq} in SMT. The exact algorithm we used to solve the 1-sparse dictionary learning problem is in Algorithm 1. Notice that when data is uniformly distributed on the domain, even a dictionary consisting of uniformly sampled data point serve as a good enough approximation. This is the case for the toy example in Figure 2. In this case, the dictionary Φ can be predefined instead of learned. For MNIST and CIFAR10 data, they are both assumed to be low dimensional data manifolds in high dimensional space. Thus, we cannot apply k-mean directly to the raw signal due to the high dimensionality and sparsity of the data. One way to alleviate this problem is to map the data to a unit sphere before applying k-mean. This method is called spherical k-mean. More detailed motivations and advantages of this approach are explained in the original paper [28]. The exact algorithm is also described in Algorithm 1.

Algorithm 1: Online 1-sparse dictionary learning heuristic (K-mean clustering)

Data: Data matrix $X = [\vec{x}_1, \dots, \vec{x}_N]$, η is learning rate.

Result: Dictionary (centroid) $\Phi = [\vec{\phi}_1, \dots, \vec{\phi}_K]$, where each column is a dictionary element

Sparse code (label) $A = [\vec{\alpha}_1, \dots, \vec{\alpha}_N]$ for each data point.

```

1 initialization:  $\Phi \leftarrow 0, A \leftarrow 0$ ;
2 if spherical then
3   for  $i \in 1, \dots, n$  do
4      $\vec{x}_i = \frac{\vec{x}_i}{\|\vec{x}_i\|_2}$ 
5   end
6 end
7 while not  $\phi$  has not converge do
8   Find the sparse code for every data point;
9   for  $i \in 1, \dots, n$  do
10     $\vec{\alpha}_i \leftarrow \vec{e}_{j^*} \quad j^* = \arg \max_j \|\vec{\phi}_j - \vec{x}_i\|$ 
11  end
12  Dictionary update;
13   $\Phi \leftarrow \Phi + \frac{\eta}{h} \odot \sum_i (\vec{x}_i - \Phi^T \vec{\alpha}_i), \quad s.t. \quad \vec{h}_j = (\sum_i \vec{\alpha}_i)_j$ ;
14  if spherical then
15    for  $j \in 1, \dots, K$  do
16       $\vec{\phi}_j = \frac{\vec{\phi}_j}{\|\vec{\phi}_j\|_2}$ 
17    end
18  end
19 end

```

E ABLATION

Since SMT is a white box model, we can analyze how each component of SMT contributes to unsupervised learning. Specifically, we break down SMT into two components: dimensionality expansion using sparse features and dimensionality reduction through spectral embedding. We first show that sparse feature by itself is important in building a good representation. As shown in Figure 6, we’re able to achieve 71 % evaluation accuracy using only sparse features (f_{gq}) on the CIFAR10 dataset. Combining sparse features with whitening will further boost the performance to 75 %. However, the performance does not increase as the number of features increases if we’re using only sparse features and whitening. In contrast, if we combine sparse feature and spectral embedding, we do see the performance increase as the number of features increases. This result implies the spectral embedding is also a crucial element to obtain a good representation.

To further show the necessity of spectral embedding, we did an experiment to replace spectral embedding with PCA. PCA is a dimension reduction algorithm but does not enforce locality. In Figure 6(b), we see that if we’re using PCA as dimension reduction, the performance decreases monotonically as we reduce the sparse feature to a lower dimension, which implies it is throwing away useful information. On the other hand, for SMT, the performance first increases and then decreases, as we increase the reduction dimension. The performance of SMT peaks when we use 500 as the

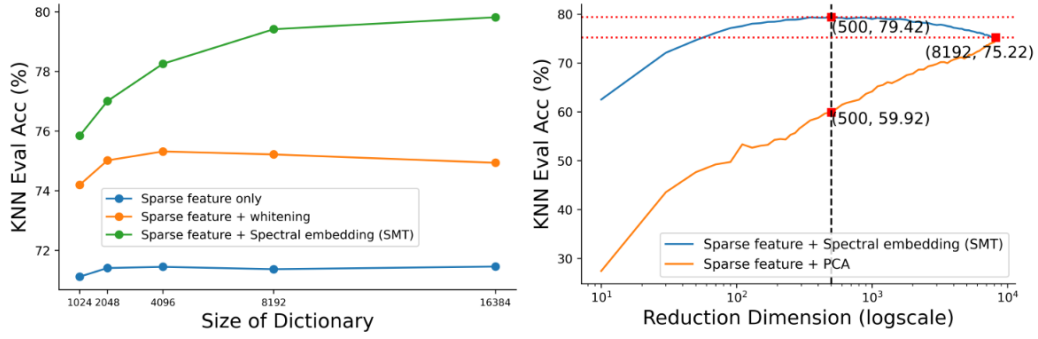


Figure 6: **Ablation Studies.** (a) Evaluation accuracy as a function of dictionary sizes on CIFAR10 dataset. We tried three representations for ablation study purpose. (b) Evaluation accuracy as a function of reduction dimension on CIFAR10 dataset. Reduction dimension corresponds to number of principle components in PCA and embedding dimension in SMT. A dictionary of size 8192 is used to build representation in this experiment.

reduction dimension, which is much higher than PCA (79.4% vs 59.9%) with 500 components and even higher than PCA with all principle components (79.4% vs 75.2%).